Comput Mech
DOI 10.1007/s00466-007-0181-y

ORIGINAL PAPER

# Combining topological sensitivity and genetic algorithms for identification inverse problems in anisotropic materials

**Lucía Comino · Rafael Gallego · Guillermo Rus**

Received: 6 February 2006 / Accepted: 4 April 2007


**Abstract** The identification inverse problem is solved here for flaw detection in anisotropic materials by means of an innovative approach: the combination of Genetic Algorithm and the *Topological Sensitivity* in anisotropic elasticity. The Topological Sensitivity provides a measure of the susceptibility of a defect being at a given location. This is based on a linearized topological expansion, applying Boundary Integral Equations and using solely information of the non-damaged state. It is proved that the Topological Sensitivity provides an accurate tool for estimating the location and size of defects. First, it is shown that the minimum of the residual (cost function) topological sensitivity pinpoints the location and size of the actual flaws, and secondly, the minimization of the residual topological sensitivity is carried out using Genetic Algorithm. When the Genetic Algorithm is applied to the residual Topological Sensitivity instead of to the full residual, the applicability of this method is enhanced since the computational effort, which is the major drawback of this type of search methods, is drastically reduced. In this paper, the formulation for linearly anisotropic elastic media is composed for the case of circular flaws, although the procedure is extensible to other kinds of defects like elliptical cavities, elastic or rigid inclusions or cracks.

**Keywords** Topological sensitivity (TS) · Genetic algorithms (GA) · Two-dimensional anisotropic elasticity · Flaw identification · Boundary integral equation (BIE) · Identification inverse problem (IIP)

L. Comino · R. Gallego · G. Rus (✉)
Department of Structural Mechanics,
University of Granada, 18071, Granada, Spain
e-mail: grus@ugr.es

R. Gallego
e-mail: gallego@ugr.es

## 1 Introduction

Identification inverse problems are usually tackled considering the problem as the minimization of a residual functional with respect to selected shape parameters. Here, a different and novel approach is employed, making use of a domain function, the so-called *Topological Sensitivity* (TS). Eschenauer et al. [2] were the first to develop the idea of TS for compliance minimization problems. Later, it was generalized and exploited for shape inverse problems by Sokołowski and co-workers [6,10]. Garreau et al. [4] generalized the idea for an arbitrarily-shaped flaw in elastostatics. The Adjoint variable method was used in all these works for the computation of the topological derivative. However, Gallego and Rus [3] first proposed a different approach, fully based on a linearized topological expansion using Boundary Integral Equation (BIE) techniques. It has been proved that the minimum of the residual topological sensitivity pinpoints the location and size of the unknown flaw.

On the other hand, gradient-based minimization procedures are generally used for identification inverse problems, mainly due to the high computational effort needed for global methods such as Genetic Algorithm (GA). The use of GA for identification of flaws within the framework of Boundary Integral Equation procedures, has been explored by different authors in the past decade. Koguchi and Watabe [7], Kowalckzyk et al. [8], Tanaka and Nakamura [15], Stavroulakis and Antes [13,14], or Stavroulakis [12] represent a good part of the works. In all these papers the functional to be optimized is the full residual. Hence, the computation is very costly. However, the computation of the residual topological sensitivity involves solely information of the non-damaged state (NS), and therefore, the location of its minimum using GA drastically reduces the computational cost as shown in [3].

The formulation for linearly anisotropic elastic media with circular flaws is built in this paper, although the procedure is extensible to other arbitrarily shaped cavities or cracks. The TS is shown to provide an accurate tool for estimating the location and size of the defect.

## 2 Topological sensitivity

The topological derivative of a shape functional can be defined as the variation of the functional due to creation of a small hole centered at a given location $x_0$. Formally, given a shape functional

$$\mathcal{J} : \Omega \to \mathcal{R} \tag{1}$$

for a given domain $\Omega$, where $B_r(x_0)$ is a closed ball of radius $r > 0$ centered at $x_0$, the topological derivative is defined as

$$\mathcal{J}^*(x_0) = \lim_{r \to 0^+} \frac{\mathcal{J}(\Omega \setminus B_r(x_0)) - \mathcal{J}(\Omega)}{\| B_r(x_0) \|} \tag{2}$$

For plane problems, such as those in this study, another definition comes from the linearized expansion of the functional $\mathcal{J}$ in the non-damaged state, around $r = 0^+$

$$J(r) = J(0^+) + \frac{r^2}{2} J''(0^+) + o(r^2) \tag{3}$$

where, if higher order terms are neglected, $J''(0^+)$ is equivalent to the topological sensitivity of the cost functional, $\mathcal{J}^*(x_0)$.

### 2.1 Topological sensitivity boundary integral equation

The objective is to solve an identification inverse problem using the topological sensitivity of a cost functional. This functional depends on the variables of the elastostatic problem: displacements and/or tractions. The formulation used for its computation starts from the Boundary Integral Equation (BIE) of the displacements [1], and once the TS of the boundary variables has been calculated, the TS of the functional can be obtained immediately.

Formally, the problem is defined first in a non-isotropic homogeneous domain $\Omega$, with boundary $\Gamma$, where there is no defect, i.e., the *non-damaged state*, subject to some boundary conditions. The displacements BIE can be written as follows:

$$c_k^i(\mathbf{y}) u_k(\mathbf{y}) + \int_\Gamma \left[ q_k^i(\mathbf{x};\mathbf{y}) u_k(\mathbf{x}) - u_k^i(\mathbf{x};\mathbf{y}) q_k(\mathbf{x}) \right] d\Gamma(\mathbf{x}) = 0 \tag{4}$$

where

- $u_k(\mathbf{x})$ is the $k$-th component of the displacement vector in the *non-damaged state* at the *observation point* $\mathbf{x}$.
- $q_k(\mathbf{x}) = \sigma_{jk}(\mathbf{x}) n_j(\mathbf{x})$ is the traction vector in the *non-damaged state*, at *observation point* $\mathbf{x}$. $\sigma_{jk}(\mathbf{x})$ is the stress tensor and $n_j(\mathbf{x})$ the outward normal.
- $u_k^i(\mathbf{x};\mathbf{y})$ is the $k$th component of the displacement vector at the *observation point* $\mathbf{x}$ due to a point load applied in direction $i$ at the *collocation point* $\mathbf{y}$. $u_k^i(\mathbf{x};\mathbf{y})$ is the displacement field of the *fundamental solution*.
- $q_k^i(\mathbf{x};\mathbf{y}) = \sigma_{lk}^i(\mathbf{x};\mathbf{y}) n_l(\mathbf{x})$ is the traction vector of the *fundamental solution*.
- $c_k^i(\mathbf{y})$ is the free term whose value depends on the position of the *collocation point* $\mathbf{y}$.

The displacements and tractions of the *fundamental solution* for the anisotropic medium can be found in [11],

$$u_j^i(\mathbf{x};\mathbf{y}) = 2\mathbf{Re}\left[ p_{j1} A_{i1} \ln(x_1 - y_1) + p_{j2} A_{i2} \ln(x_2 - y_2) \right] \tag{5}$$

$$q_j^i(\mathbf{x};\mathbf{y}) = 2\mathbf{Re}\left[ \frac{q_{j1} A_{i1}}{x_1 - y_1} (\mu_1 n_1 - n_2) + \frac{q_{j2} A_{i2}}{x_2 - y_2} (\mu_2 n_1 - n_2) \right]$$

$A_{ij}$, $p_{ij}$ and $q_{ij}$ are functions of the material elastic constants $a_{ij}$[1] and $x_k$ is the complex variable, $x_k = x_1 + \mu_k x_2$, being $\mu_k$ the complex roots of the characteristic Eq. ([9]):

$$l_4(\mu) = \beta_{11}\mu^4 - 2\beta_{16}\mu^3 + (\beta_{12} + \beta_{66})\mu^2 - 2\beta_{16}\mu + \beta_{22} \tag{6}$$

where $\beta_{ij}$ are called *reduced elastic constants*; for the plane strain state they are defined as follows $\beta_{ij} = a_{ij} - (a_{i3}a_{j3})/a_{33}$. Equation (4) is discretized and can be solved with standard Boundary Element techniques. Then, with the kinematic equations and Hooke's law, the rest of the variables of the problem in the domain $\Omega$ and on its boundary $\Gamma$ are obtained.

The next step is to consider a modified state that contains an vanishing flaw, the *damaged state*. In the same homogeneous domain $\Omega$, whose exterior boundary is $\Gamma$, and subject to the same boundary conditions, consider the appearance of a traction-free cavity centered at point $\mathbf{z}$ whose boundary is $\Gamma_z$, which surrounds the domain $\Omega_z$. The BIE for displacements in the new state is written as follows, where the boundary has

[1] Hooke's law $\varepsilon_i = a_{ij}\sigma_j \quad i, j = 1 \ldots 6$

been split into $\Gamma$ and $\Gamma_z$,

$$c_k^i(\mathbf{y})\tilde{u}_k(\mathbf{y}) + \int_\Gamma \left[q_k^i(\mathbf{x};\mathbf{y})\tilde{u}_k(\mathbf{x}) - u_k^i(\mathbf{x};\mathbf{y})\tilde{q}_k(\mathbf{x})\right] d\Gamma(\mathbf{x}) + \int_{\Gamma_z} \left[q_k^i(\mathbf{x};\mathbf{y})\tilde{u}_k(\mathbf{x}) - u_k^i(\mathbf{x};\mathbf{y})\tilde{q}_k(\mathbf{x})\right] d\Gamma(\mathbf{x}) = 0 \tag{7}$$

where the tilde over the variables means that their values are modified due to the appearance of the vanishing flaw. Equation (7) can be simplified considering several reasons. First, $\tilde{q}_k = 0$ along $\Gamma_z$, since the cavity boundary is traction-free. Next, the displacements along the defect boundary $\Gamma_z$ can be expressed as the sum of a rigid body motion plus a movement relative to the center.

$$\tilde{u}_k(\mathbf{x}) = u_k^0 + \delta\bar{u}_k(\mathbf{x}) \tag{8}$$

Moreover, stresses at a point $\mathbf{y}$ interior to the domain $\Omega\backslash\Omega_z$, far from the defect, are similar to the ones in the non-damaged state $\sigma_{ij}(\mathbf{z})$ (up to first order terms). Therefore, the displacements $\delta\bar{u}_k(\mathbf{x})$ along the boundary defect $\Gamma_z$ are equal to those in an infinite domain subject to a uniform remote stress field $\sigma_{ij}(\mathbf{z})$, $\delta u_k^\infty(\mathbf{x})$, i.e.,

$$\tilde{\sigma}_{ij}(\mathbf{y}) = \sigma_{ij}(\mathbf{y}) + h.o.t. \tag{9}$$

$$\delta\bar{u}_k(\mathbf{x}) = \delta u_k^\infty(\mathbf{x}) + h.o.t. \tag{10}$$

where $h.o.t.$ stands for *higher order terms*.

Finally, on the boundary of the cavity,

$$q_k^i(\mathbf{x};\mathbf{y}) = \sigma_{jk}^i(\mathbf{x};\mathbf{y})n_j(\mathbf{x}) = \sigma_{jk}^i(\mathbf{z};\mathbf{y})n_j(\mathbf{x}) + h.o.t. \tag{11}$$

Taking everything into account and subtracting the BIE for the non-damaged state, Eq. (4), to the BIE for the damaged state, Eq. (7), the so-called Topological Sensitivity Boundary Integral Eq. (TSBIE) is obtained (see [3] for a more detailed description of the process), namely,

$$c_k^i(\mathbf{y})\delta u_k(\mathbf{y}) + \int_\Gamma \left[q_k^i(\mathbf{x};\mathbf{y})\delta u_k(\mathbf{x}) - u_k^i(\mathbf{x};\mathbf{y})\delta q_k(\mathbf{x})\right] d\Gamma(\mathbf{x}) = -\sigma_{jk}^i(\mathbf{z};\mathbf{y}) \int_{\Gamma_z} n_j(\mathbf{x})\delta u_k^\infty(\mathbf{x}) d\Gamma(\mathbf{x}) \tag{12}$$

where $\delta u_k(\mathbf{y})$ and $\delta q_k(\mathbf{y})$ are the topological sensitivities of displacements and tractions on the boundary due to the appearance of an infinitesimal arbitrarily shaped flaw at $\mathbf{z}$.

### 2.2 Topological sensitivity BIE for circular cavities

For the case of defects modeled as circular cavities with radius $\delta R$, traction-free boundaries in an anisotropic medium, the displacements $\delta u_k^\infty(\mathbf{x})$ have analytical expressions that can be written in the form

$$\delta u_k^\infty = -\delta R\, \Sigma_{kl} n_l \tag{13}$$

for $k, l = 1, 2$, where $n_l$ is the outward normal to the boundary $\Gamma_z$ and $(\Sigma_{kl})$ is a constant matrix which depends on the value of $\sigma_{ij}(\mathbf{z})$, the elastic constants $a_{ij}$ and the complex roots $\mu_i$. In particular, the component $\Sigma_{11}$ is computed as follows (the value of rest of the components is detailed in the Appendix),

$$\begin{aligned}\Sigma_{11} = \frac{1}{|\mu_1-\mu_2|^2}\big[&a_{11}(\mathbf{Im}(\mu_1+\mu_2)(\mathbf{Im}^2(\mu_1) \\ &-2\mathbf{Im}(\mu_1)\mathbf{Im}(\mu_2) + \mathbf{Im}^2(\mu_2) + \mathbf{Re}^2(\mu_1-\mu_2))\sigma_{11} \\ &+ |\mu_1-\mu_2|^2\,(\sigma_{11} + \mathbf{Re}(\mu_2)\sigma_{12} \\ &+\mathbf{Im}(\mu_1)\mathbf{Re}(\mu_2)\sigma_{12} - \mathbf{Im}(\mu_1)\mathbf{Im}(\mu_2)\sigma 22 \\ &+\Re(\mu_1)(\sigma 12 + \mathbf{Im}(\mu_2)\sigma 12 + \mathbf{Re}(\mu_2)\sigma 22)))\big]\end{aligned} \tag{14}$$

Finally, if Eq. (13) is substituted into the TSBIE (12), then

$$c_k^i(\mathbf{y})\delta u_k(\mathbf{y}) + \int_\Gamma \left[q_k^i(\mathbf{x};\mathbf{y})\delta u_k(\mathbf{x}) - u_k^i(\mathbf{x};\mathbf{y})\delta q_k(\mathbf{x})\right] d\Gamma(\mathbf{x}) = -\pi\delta R^2\, \sigma_{jk}^i(\mathbf{z};\mathbf{y})\Sigma_{kl}(\mathbf{z})\delta_{jl} = -\delta A\, \sigma_{jk}^i(\mathbf{z};\mathbf{y})\Sigma_{kj}(\mathbf{z}) \tag{15}$$

where $\delta A = \pi\delta R^2$ is the area of the circular cavity.

When the TSBIE (12) is generalized for $m$ circular cavities centered at a set of points $\mathbf{z}^l$, the right hand side of the Eq. (15) becomes $\sum_{l=1}^m {}^tU^i(\mathbf{z}^l;\mathbf{y})\delta A_l$, where $\delta A_l$ is a vector containing the areas of each of the flaws centered at $z^l$, and ${}^tU^i(\mathbf{z}^l;\mathbf{y}) = \sigma_{jk}^i(\mathbf{z}^l;\mathbf{y})\Sigma_{kj}(\mathbf{z}^l)$.

### 2.3 Discretization and solution of topological sensitivity BIE

In order to solve the TSBIE, standard discretization techniques based on the Boundary Element Method are employed, obtaining an algebraic system of equations:

$$\mathbf{M}\delta\mathbf{v} = {}^t\mathbf{\Delta}\delta\mathbf{A} \tag{16}$$

where $\delta\mathbf{v}$ is a vector with the sensitivities of the corresponding unknowns variables on the boundary (displacements and/or tractions); $\delta\mathbf{A}$ is a vector with the areas of the defects and ${}^t\mathbf{\Delta}$ is a matrix $n \times m$ where $n$ is the number of collocation points and $m$ is the number of defects.

Since the integral operator of $\delta u_k$ and $\delta q_k$ in Eq. (12) is equal to the one of $u_k$ and $q_k$ in Eq. (4), then, the coefficient matrix $\mathbf{M}$ is the same for both problems, and therefore, once the non-damaged state is discretized and its matrix system factorized, boundary sensitivities can be obtained by simple forward-backward substitution. Doing so for each column of ${}^t\boldsymbol{\Delta}$, the *Topological Jacobian* is obtained, defined as,

$$\mathbf{M}\,{}^t\mathbf{J} = {}^t\boldsymbol{\Delta}. \tag{17}$$

Hence, the topological sensitivities of the boundary variables can be computed by,

$$\delta\mathbf{v} = {}^t\mathbf{J}\delta\mathbf{A} \tag{18}$$

## 3 Defect identification with the topological sensitivity

As mentioned above, the inverse problem for defect identification is usually tackled as the minimization of a cost functional, which represents the difference between the measured values of a physical magnitude (for instance displacements, tractions or strains) and the computed ones in an assumed configuration. It will be shown here how the minimum of the TS of the cost functional pinpoints the location and size of the unknown flaw. This entails a great saving in computational effort, since, for a given location of the flaws, the problem can be solved using only the solution of the non-damaged state. Hence, the flaw discretization is avoided.

### 3.1 Defect size estimation

The first step of the proposed strategy is the defect size calculation. The cost functional is defined as $f = \frac{1}{2}\mathbf{R}^T\mathbf{R}$, where $\mathbf{R}$ is the residual vector defined from the discrepancy between a certain experimentally measured magnitude $\mathbf{v}^{\exp}$ (displacements and/or tractions), and its value computed with the assumed model with $m$ flaws centered at $\mathbf{z}^l$, $\mathbf{R} = \mathbf{v}^{\exp} - \mathbf{v}(\mathbf{A}(\mathbf{z}^l))$. Using the topological expansion for the residual $\mathbf{R}$ in a non-damaged state and taking into account Eq. (18),

$$\mathbf{R}(\mathbf{A}(\mathbf{z}_j)) \cong \mathbf{v}^{\exp} - (\mathbf{v}(0) + \delta\mathbf{v}) = \Delta\mathbf{v} - {}^t\mathbf{J}(\mathbf{z}_j)\delta\mathbf{A} \tag{19}$$

where $\Delta\mathbf{v} = \mathbf{v}^{\exp} - \mathbf{v}(0)$ can be computed once the non-damaged state is solved. Applying the topological expansion of $\mathbf{R}$ to the functional definition, $f$ is approximated by

$$\begin{aligned} f &= \frac{1}{2}\mathbf{R}^T\mathbf{R} \cong f(0) + \delta f \\ &= f(0) + \frac{1}{2}\delta\mathbf{A}^T\,{}^t\mathbf{J}^T\,{}^t\mathbf{J}\,\delta\mathbf{A} - \delta\mathbf{A}^T\,{}^t\mathbf{J}^T\,\Delta\mathbf{v} \end{aligned} \tag{20}$$

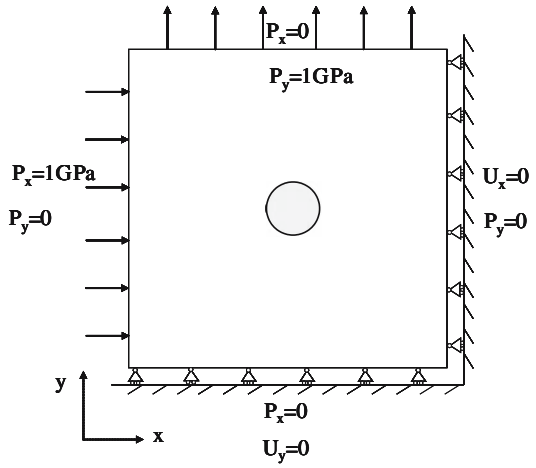


**Fig. 1** Geometry of benchmark problem

where $f(0) = \frac{1}{2}\Delta\mathbf{v}^T\Delta\mathbf{v}$, and $\delta f$ is the *topological sensitivity of the cost functional*. The optimum sizes of the possible flaws will be those which minimizes the cost functional TS (20), i.e.,

$$\delta\mathbf{A} = ({}^t\mathbf{J}^T\,{}^t\mathbf{J})^{-1}\,{}^t\mathbf{J}^T\,\Delta\mathbf{v} \tag{21}$$

Note that ${}^t\mathbf{J}^T\,{}^t\mathbf{J}$ is a small $m \times m$ matrix, so its inversion is computationally inexpensive.

This idea has been validated with a simple benchmark problem (see Fig. 1). The example consists of a square plate, 2m × 2m, made of an orthotropic material (birch plywood). The plate, which is subject to the boundary conditions of the figure, has a centered circular cavity, and its boundary is discretized into 80 quadratic isoparametric elements.

The experimental data needed to compute the residual $\mathbf{R}$ have been simulated solving the direct problem with a Fortran code in a damaged plate with a circular cavity modeled with 48 elements. The problems have been solved for different radii $r$ of the flaw, from a small one, $r \approx 10^{-6}$ m, to a large one $r \approx 0.8$ m. Note that in the last case the cavity occupies almost the whole domain.

The real radius has been plotted versus the one obtained with the topological sensitivity and Eq. (21) in Fig. 2. The correlation is nearly one to one, with discrepancies only when flaw almost occupies the whole plate. These errors are due to the influence of neglected higher order terms in the expansions.

### 3.2 Location of the defect

Once the defect size has been estimated with Eq. (21), the linearized approximation of the functional is obtained by applying Eq. (20),

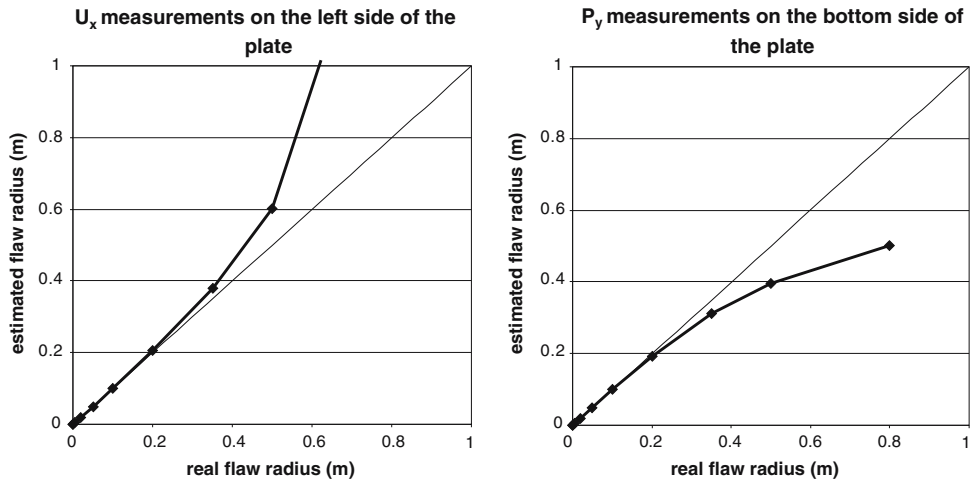


**Fig. 2** Correlation between estimated and real radius of the cavity

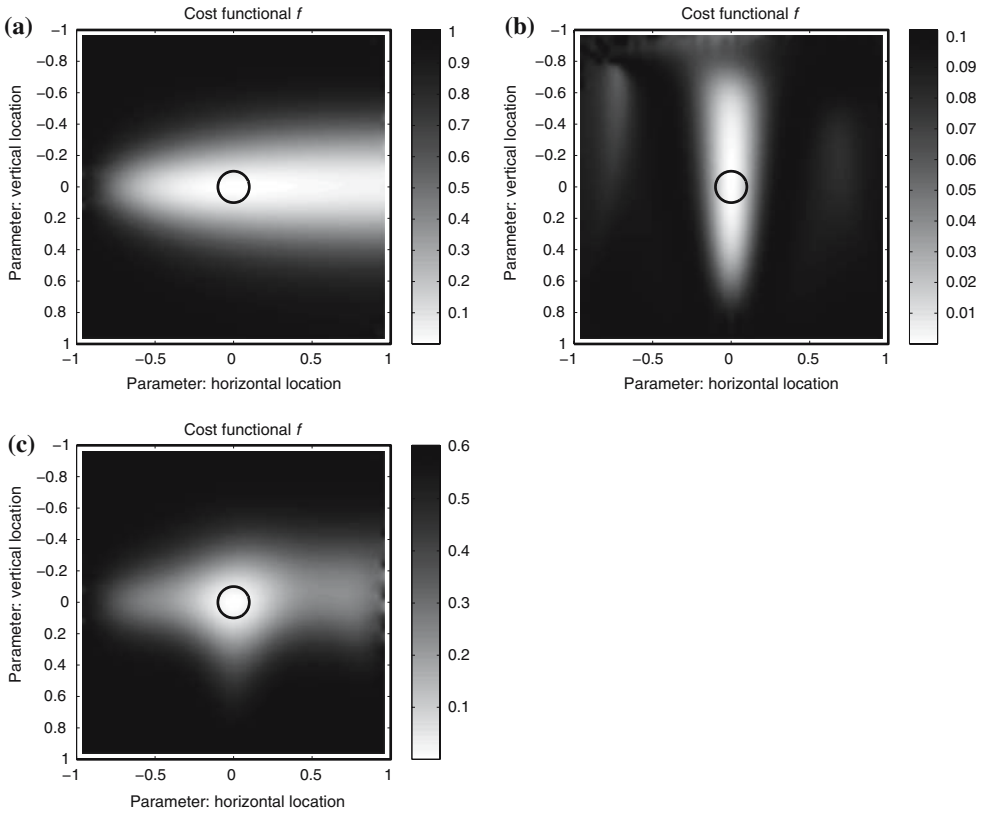


**Fig. 3** Cost Functional for a centered circular cavity. Experimental data: **a** $U_x$ on *left plate side* **b** $P_y$ on *bottom plate side* **c** $U_x$ on *left plate side* + $P_y$ on *bottom plate side*

$$f \cong f(0) + \delta f(\mathbf{z}^l) = (\Delta\mathbf{v} - {}^t\mathbf{J}(\mathbf{z}^l)\delta\mathbf{A})^T(\Delta\mathbf{v} - {}^t\mathbf{J}(\mathbf{z}^l)\delta\mathbf{A}) \tag{22}$$

The centers of the defects will be located at the points $\mathbf{z}^l$ which minimize the value of $f$, or using the topological expansion, at the points such that $\delta!f$ attains its minimum.

Several tests were run using the example in Fig. 1, having fixed the radius of the actual cavity to $r = 0.1$m. The results are shown in next figures where the cost functional, computed with the linearized expansion and the topological sensitivity in Eq. (20), is plotted and superimposed on the real geometry of the domain and location of the flaws (thick line). The optimum flaw predicted by minimizing the cost functional TS is represented as well (thin line).

Three cases are shown in Fig. 3, differing in the experimental data used to compute the functional. The actual and predicted flaws are indistinguishable, which confirms that the minimum of the cost functional TS pinpoints, not only the

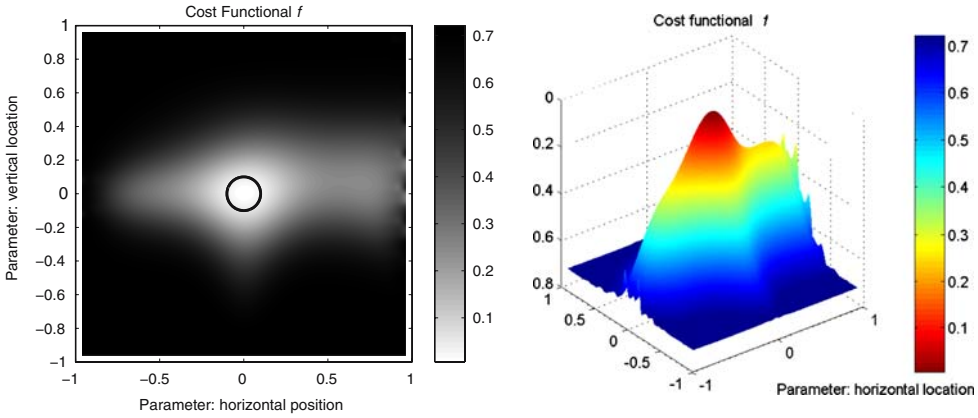


**Fig. 4** Cost Functional topological expansion in the domain for a centered circular cavity with 10% error in the elastic constants

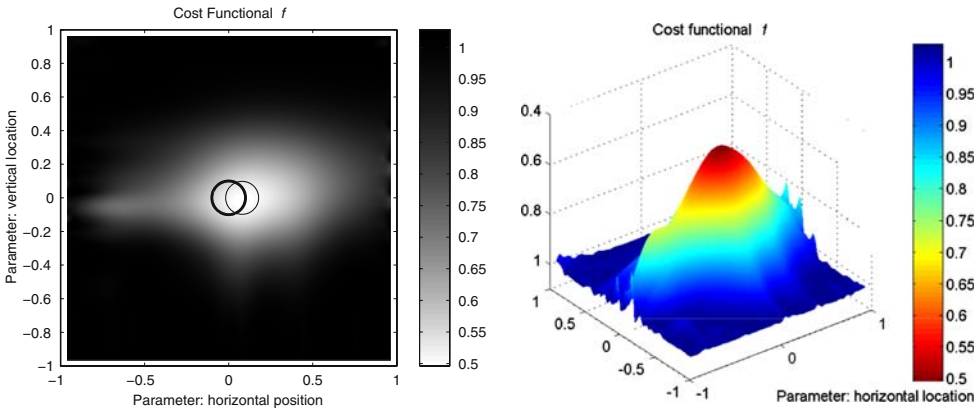


**Fig. 5** Cost Functional topological expansion in the domain for a centered circular cavity with 5% error in simulated experimental data

size, but the presence and location of the cavity. It can be appreciated that the greater the amount of experimental data, the more accurately the location of the cavity is identified. It should be pointed out that the minimum value is attained at the center, and moreover, it is three orders of magnitude smaller than its value elsewhere, indicating the location of the flaw.

To verify the stability of the method, simulated errors are introduced. First, the elastic constants of the material are disturbed with a percentage of Gaussian random noise computationally generated. Even with a large amount of noise, 10% of Gaussian error, the minimum of the cost functional, 100 times smaller than elsewhere, pinpoints accurately the center of the flaw, (Fig. 4). The radius is also well estimated. Second, an error is introduced in the experimental measurements. Although not as accurate as in previous cases, with a 5% of noise in the data, the minimum of the cost functional TS is close to the exact position of the center, and the size of the cavity is well predicted, (Fig. 5).

Finally, a problem with a modeling error is presented. In this case the real flaw is a centered ellipse whose half-axes are $a = 0.15$m and $b = 0.1$m. The boundary conditions are the same as in previous applications. The topological sensitivity is computed considering that the flaw is a circular cavity. The location and size of the defect is still well predicted (see Fig. 6). The value of the minimum of the cost functional is half of the value elsewhere.

## 4 Genetic algorithms combined with topological sensitivity

The identification of flaws by Genetic Algorithms using BIE has been proposed by a number of authors, as mentioned in the Introduction. The Genetic Algorithms are zero-order methods, i.e. do not use information about the sensitivity or gradient of the cost functional with respect to the design parameters, and are therefore well suited for problems where this gradient is unavailable, or is expensive to compute.

Most of the authors have employed this type of algorithms to minimize the full cost functional. Instead of that, it has been shown above that the minimum of the cost functional topological sensitivity pinpoints accurately the location and size of the defect. Since Genetic Algorithms are global zero-order methods, there is no need to compute the gradient of the functional with respect the unknowns of the problem. This is an important advantage, but as a counterpart, the computational

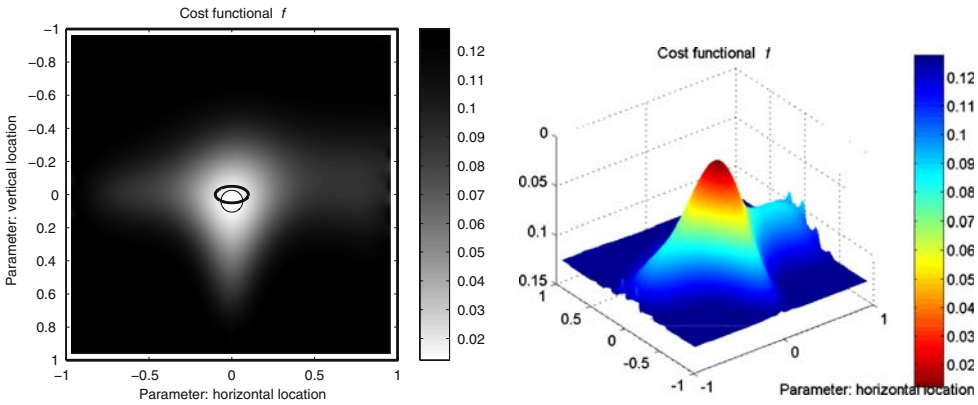


**Fig. 6** Cost Functional topological expansion in the domain for a centered elliptic cavity

effort is high, since a large number of direct problems has to be evaluated and solved.

The use of the cost functional topological sensitivity, instead of the full functional, drastically reduce this computational time, since the solution of the problems with flaws is found using only information of the non-damaged state, and no flaw discretization is needed. Moreover, the optimum size is estimated independently once the flaw centers are given, reducing the number of design parameters, which additionally accelerates the convergence of the GA.

### 4.1 Description of the genetic algorithms

Within the framework of genetic optimization, the set of design parameters, or *phenotype*, is encoded as a chain of variables, *chromosomes*. A population of *individuals*, is assumed.

For the present study, each *individual* of the population consists of $2 \times m$ design parameters, which are the coordinates of the defect centers. For each individual a *fitness function* defined as $e(\mathbf{x}) = -\log f(\mathbf{x})$ is computed, where $f(\mathbf{x})$ is the cost functional topological sensitivity, and $\mathbf{x}$ the design parameters.

The simulation is carried out with the following steps:

1. The non-damaged state is solved. The system matrix $\mathbf{M}$ is factorized and the vector $\Delta v$ (Eq. 19) is evaluated.
2. A random population of individuals (flaw centers) is generated.
3. For each individual:
   (a) The matrix $\Delta$ (Equation 16) is computed. In order to evaluate this matrix, the stress tensor at the centers of the flaws *for the ND state* is computed.
   (b) The topological Jacobian is computed, by back and forward substitution, solving the system (17).
   (c) Optimum flaw sizes ($\delta A$) are computed using Eq. (21)
   (d) The cost functional topological sensitivity is evaluated, using Eq. (22).
   (e) The fitness function for the individual is obtained by $e(\mathbf{x}) = -\log f(\mathbf{x})$.
4. Given the fitness of each individual, standard genetic operators (selection, crossover, mutation) are performed over the population, rendering a new one.
5. Steps from 3 are repeated until a stopping criteria is fulfilled.

It should be stressed out that, if minimizing the full cost funtional instead of its topological sensitivity, step 3 would entail the full solution of a damaged problem, *for each individual*. This is computationally much more expensive than the proposed algorithm.

There is a large number of variations and additions to the three basic genetic operators, but the simplest version is used in this paper, since the objective is not to test the GA, but the improvement raised out by its aplication to the topological sensitivity of the cost functional.

### 4.2 Numerical applications

To conclude, the whole strategy is going to be test with a series of applications. The code has been adapted from the one developed by Haataja [5]. The values of the different parameters which control the GA are shown in Table 1. With these parameters, using the algorithm for seeking defects by itself, would imply solving 200 times $50 = 10,000$ different direct problems with cavities. On the contrary, if the cost functional topological sensitivity is minimized, instead of

**Table 1** Genetic algorithm parameters

| Number of individuals in population | 50 |
|---|---|
| Number of generations | 200 |
| Probability of mutation | 0.02 |
| Probability of crossover | 0.8 |
| Probability of "tournament" | 0.7 |
| Scale of mutation | 0.1 |

the full cost functional, just one problem has to be solved, the non-damaged state, and each of the 10, 000 analyses involves just the computation of stresses and forward and back substitution with the already factorized system matrix **M**.

Multiple tests have been undertaken. For all of them, the studied specimen is a square plate with the same dimensions, material properties and boundary conditions as the those of the benchmark example in Fig. 1. Each of the following figures have two graphics. On the left hand side, the best individual obtained (thin line) is represented superimposed to the real flaw (thick line). The graph on the right hand side shows the evolution of the fitness function along the generations, of the best individual and the mean of the whole population.

The first group of tests consisted of a plate with a circular cavity, with several percentages of Gaussian error in the measurements, ranging from 0 to 10%. The number of allowed generations is 50. In all the cases, a good estimation of the size of the defect is obtained, and the location is well predicted with errors up to 5% (Fig. 7).

In the second test, the actual cavity is elliptical. As in the previous cases, tests with exact and noisy experimental data have been run. Although the exact shape of the actual cavity cannot be attain, the location and size of the flaw is well approximated even with a 10% of error in the measurements (see Fig. 8).

A third kind of tests is carried out where the design parameters represent two cavities. Hence, the *chromosome* has four parameters, two coordinates for each of the two centers. Two-hundred generations are permitted from now on. In Figs. 9 and 10 three cases are plotted. They differ in the number and type of measurements taken on the boundary of the plate to compute the residual **R**. No error on measurements is considered. It can be concluded that more experimental data the better the results, but the choice of where to measure appears

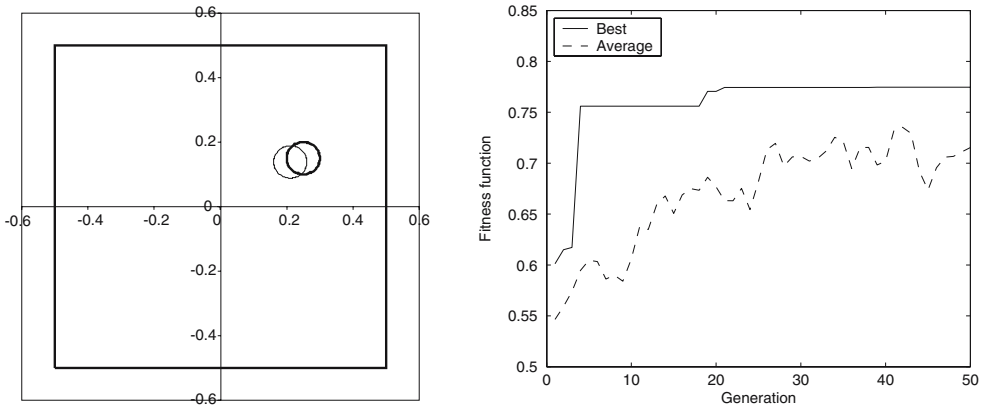


**Fig. 7** Identification of circular cavity, considering 5% error in the experimental data

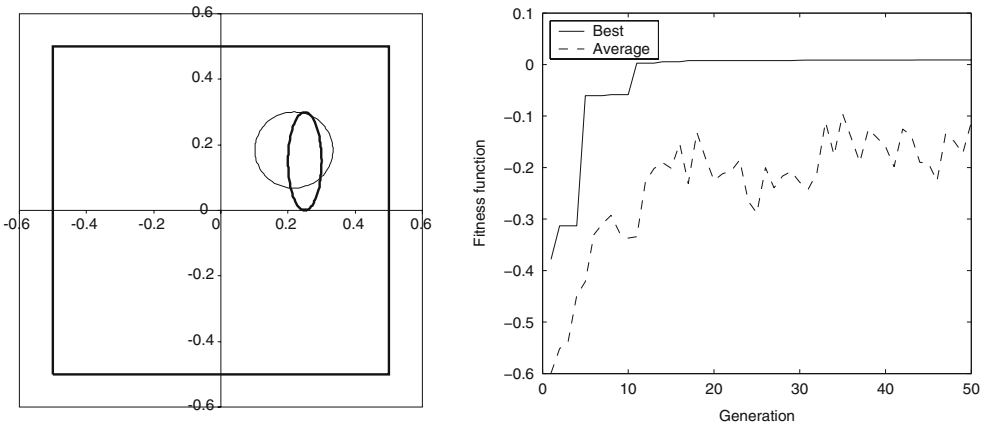


**Fig. 8** Identification of elliptic cavity, with 10% error in the experimental data

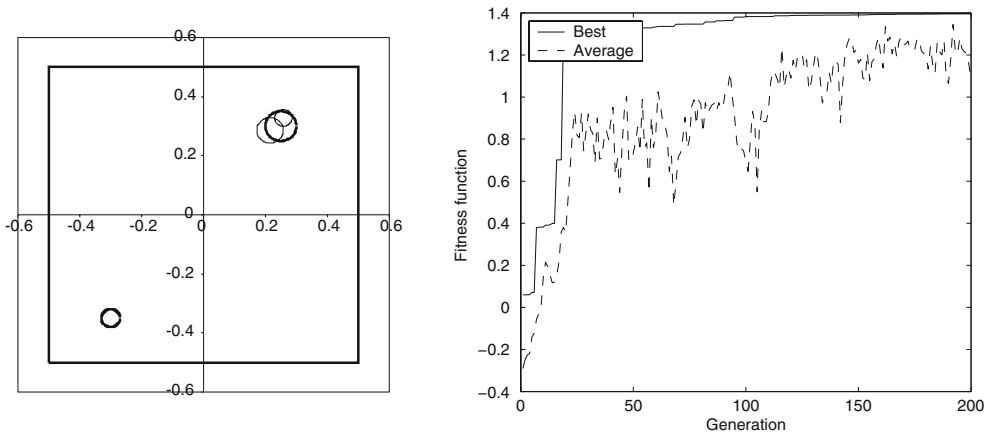


**Fig. 9** Identification of two circular cavities, with exact measurements of $P_x$ on the *right hand side* of the plate and $U_x$ on the *left hand side* of the plate

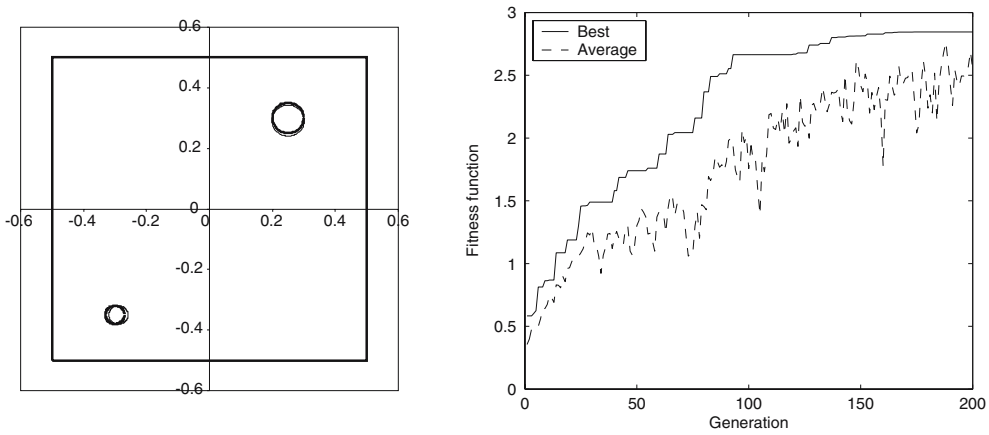


**Fig. 10** Identification of two circular cavities, with exact measurements of $U_y$ on the *top side* of the plate and $U_x$ on the *left hand side* of the plate

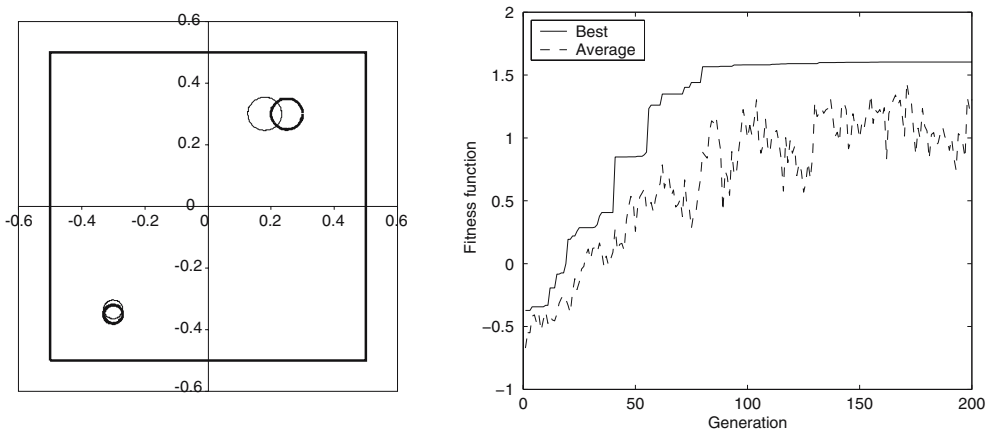


**Fig. 11** Identification of two circular cavities, with exact measurements of $P_x$ on the *right hand side* of the plate, $U_x$ on the *left hand side* of the plate, and $P_y$ at the *bottom side*

to be relevant. The case displayed in Fig. 9, just predicts one of the cavities. Figure 10 shows the best fit between predicted and real cavities, where the measurements taken are displacements $U_y$ at the top side of the plate and $U_x$ on the left hand side of the plate. Instead, in Fig. 11, tractions are measured on two sides of the plate, plus displacements in just one; in this case, the best individual fitness is lower than in Fig. 10.

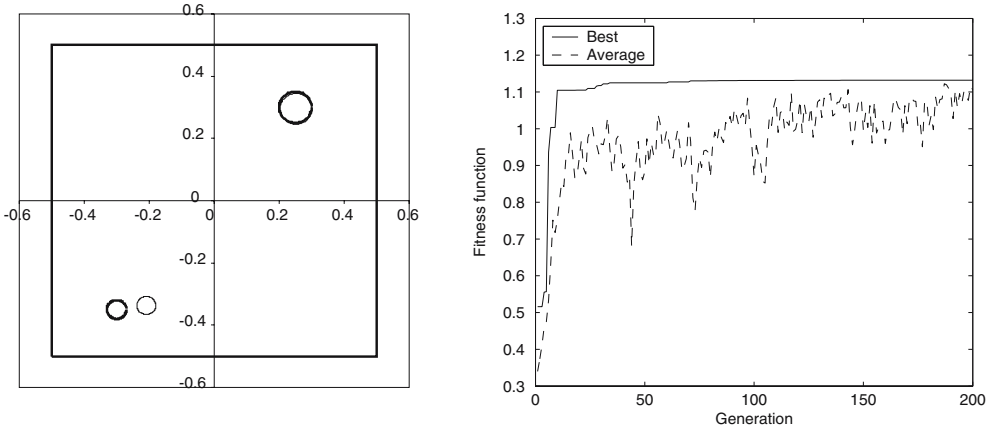


**Fig. 12** Identification of two circular cavities, with 2% error in the measurements of $U_y$ at the *top side* of the plate and $U_x$ on the *left hand side* of the plate

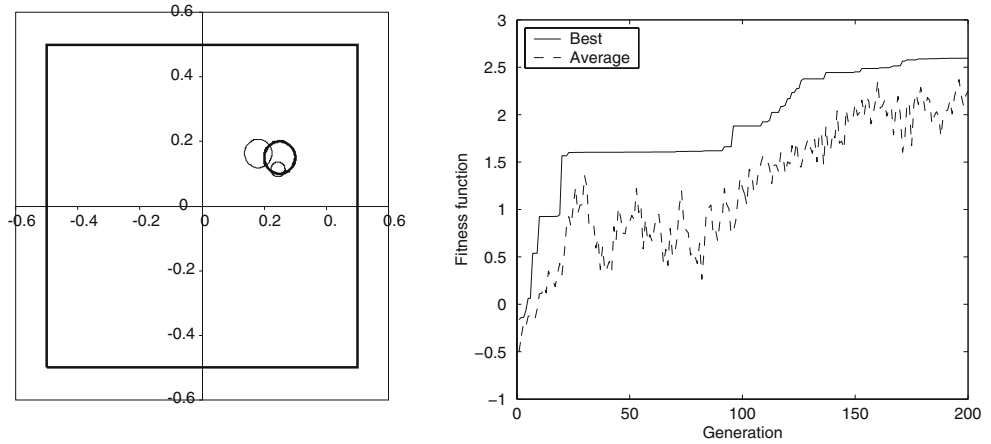


**Fig. 13** Identification of a circular cavity, allowing the existence of two circular cavities, measurements on the four sides of the plate

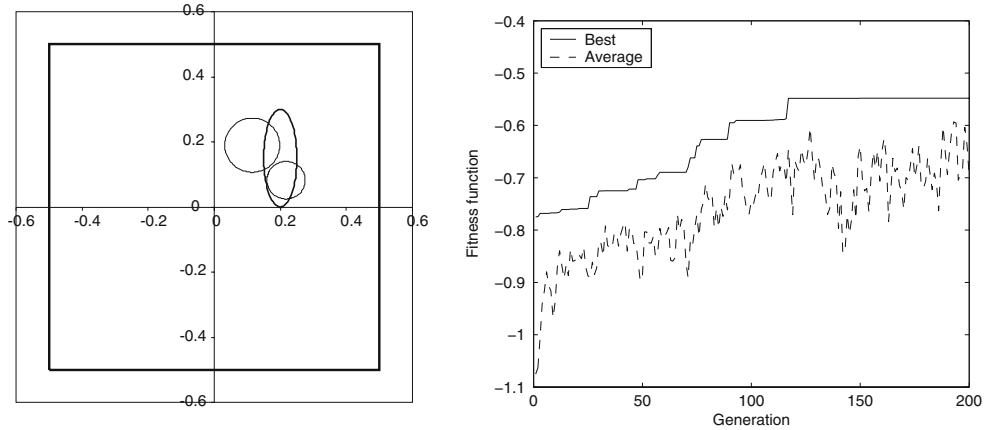


**Fig. 14** Identification of an elliptic cavity, starting from two circular cavities, with measurements on the four sides of the plate

Finally, Fig. 12 presents the results when seeking two cavities, adding 2% of noise to the measurements. One of the cavities is found accurately, while the approximation of the second one is acceptable.

Figure 13 shows the case of a single actual defect, but coding two defects in each chromosome. The result of the algorithm is that both cavities converge to the real one.

Finally, the results when two cavities are coded, but the actual defect is an elliptic cavity, are displayed in Fig. 14. Exact measurements on the four sides of the plates have been considered. The location and size are well estimated.

## 5 Conclusions

This paper confirms the efficiency of a novel strategy for identification inverse problem resolution in anisotropic materials. It combines the computation of the topological sensitivity of the cost functional with a zero order minimization algorithm. The formulation is here developed for the anisotropic case and the results of several tests verify its validity.

The TS by itself is a promising tool for identification of defects, since it provides an accurate estimate of the flaw size and its location, using only information of the flawless problem. First, the numerical results show an almost perfect correlation between the predicted and real radius of the cavity for a wide range of sizes. Then, it is demonstrated that the minimum of the topological sensitivity of the cost functional pinpoints the center of the defect, even if errors in the material properties of the model are considered, and noise is introduced into the experimental data measured on the boundary.

The major benefit of the TS comes when it is employed in conjunction with Genetic Algorithms. The disadvantages of zero-order minimization algorithms related to computational time disappear, since just the non-damaged state is solved by the BEM. Numerous applications have been performed under different conditions such as: number of actual defects, number of coded defects, kind and location of measurements, noise in the measurements, shape, size and location of the actual defect(s). The algorithm has converged to acceptable solutions under severe conditions. Some important issues should be considered in order to attain a good solution, which are the amount of experimental data, type of data, boundary where the data is collected, and size of the actual flaw.

A drawback of this algorithm in its present form is its limitation to circular shape defects. However, this limit can be overcome using available elastic solutions for other shapes such as elliptical cavities, cracks, elliptical inclusions, rigid inclusions, etc [9].

For more complex shapes a two-step approach can be devised. In the first step, a global search is performed using the present algorithm; in the second step the shape of the located defects is refined increasing the shape parameters and carrying out a local minimization of the full cost functional using a standard gradient-based algorithm. In this case, the defects found by TS-GA are plugged as an initial guess into a gradient-based algorithm.

## Appendix: Analytical expressions to compute the displacements in an infinite anisotropic domain with an uniform stress state

$$
\begin{aligned}
\Sigma_{12} = {} & \frac{a_{16}\sigma_{11}(0.5\,|\mu_1-\mu_2|^2 + \mathbf{Im}^2(\mu_1) - 2\mathbf{Im}(\mu_1)\mathbf{Im}(\mu_2) + \mathbf{Im}^2(\mu_2) + \mathbf{Re}^2(\mu_1) - 2\mathbf{Re}(\mu_1)\mathbf{Re}(\mu_2) + \mathbf{Re}^2(\mu_2))}{|\mu_1-\mu_2|^2} \\
& + \frac{|\mu_1-\mu_2|^2\,(a_{12}\sigma_{12} + 0.5(a_{66}\sigma_{12} + a_{26}\sigma_{22})) + a_{11}(-\mathbf{Re}^3(\mu_1)\sigma_{11} + \mathbf{Re}^2(\mu_1)\mathbf{Re}(\mu_2)\sigma_{11} + \mathbf{Re}(\mu_1)\mathbf{Re}^2(\mu_2)\sigma_{11}}{|\mu_1-\mu_2|^2} \\
& + \frac{-\mathbf{Re}^3(\mu_2)\sigma_{11} - \mathbf{Im}^2(\mu_1)\mathbf{Re}(\mu_1+\mu_2)\sigma_{11} - \mathbf{Im}^2(\mu_2)\mathbf{Re}(\mu_1+\mu_2)\sigma_{11} - |\mu_1-\mu_2|^2\,\mathbf{Re}(\mu_1)\mathbf{Re}(\mu_2)\sigma_{12}}{|\mu_1-\mu_2|^2} \\
& + \frac{|\mu_1-\mu_2|^2\,\mathbf{Im}(\mu_2)(\sigma_{12} + \mathbf{Re}(\mu_1)\sigma_{22}) + \mathbf{Im}(\mu_1)(\mathbf{Im}(\mu_2)(2\mathbf{Re}(\mu_1)\sigma_{11} + 2\mathbf{Re}(\mu_2)\sigma_{11} + |\mu_1-\mu_2|^2\,\sigma_{12})}{|\mu_1-\mu_2|^2} \\
& + \frac{|\mu_1-\mu_2|^2\,(\sigma_{12} + \mathbf{Re}(\mu_2)\sigma_{22})))}{|\mu_1-\mu_2|^2}
\end{aligned}
\tag{1}
$$

$$
\begin{aligned}
\Sigma_{21} = {} & \frac{0.5a_{16}\,|\mu_1-\mu_2|^2\,|\mu_1|^2\,|\mu_2|^2\,\sigma_{11} + |\mu_1-\mu_2|^2\,(0.5a_{66}\,|\mu_1|^2\,|\mu_2|^2\,\sigma_{12} + a_{12}\,|\mu_1|^2\,|\mu_2|^2\,\sigma_{12}}{|\mu_1-\mu_2|^2\,|\mu_1|^2\,|\mu_2|^2} \\
& + \frac{a_{26}(0.5\,|\mu_1|^2\,|\mu_2|^2 + |\mu_1|^2\,|\mu_2|^2)\sigma_{22}) + a_{22}(|\mu_1|^2\,(\mathbf{Im}(\mu_2)(\mathbf{Re}(\mu_1) - 2\mathbf{Re}(\mu_2)) + \mathbf{Im}(\mu_1)\mathbf{Re}(\mu_2))\sigma_{11}}{|\mu_1-\mu_2|^2\,|\mu_1|^2\,|\mu_2|^2} \\
& + \frac{|\mu_2|^2\,(\mathbf{Im}(\mu_2)\mathbf{Re}(\mu_1) + \mathbf{Im}(\mu_1) - 2(\mathbf{Re}(\mu_1) + \mathbf{Re}(\mu_2)))\sigma_{11} + |\mu_1-\mu_2|^2\,(\mathbf{Im}(\mu_1)(\mathbf{Im}(\mu_2) + |\mu_2|^2)\sigma_{12}}{|\mu_1-\mu_2|^2\,|\mu_1|^2\,|\mu_2|^2} \\
& + \frac{\mathbf{Im}^2(\mu_1)(\mathbf{Im}(\mu_2)\sigma_{12} - \mathbf{Re}(\mu_2)\sigma_{22}) + \mathbf{Re}(\mu_1)(\mathbf{Im}(\mu_2)\mathbf{Re}(\mu_1)\sigma_{12} - \mathbf{Im}^2(\mu_2)\sigma_{22} - \mathbf{Re}(\mu_2)(\sigma_{12} + \mathbf{Re}(\mu_1+\mu_2))\sigma_{22})))}{|\mu_1-\mu_2|^2\,|\mu_1|^2\,|\mu_2|^2}
\end{aligned}
\tag{2}
$$

$$
\begin{aligned}
\Sigma_{22} = & \frac{a_{12}\,|\mu_1|^2\,|\mu_2|^2\,(|\mu_1-\mu_2|^2 - \mathbf{Im}^2(\mu_1) + 2\mathbf{Im}(\mu_1)\mathbf{Im}(\mu_2) - \mathbf{Im}^2(\mu_2) - \mathbf{Re}^2(\mu_1) + 2\mathbf{Re}(\mu_1)\mathbf{Re}(\mu_2) - \mathbf{Re}^2(\mu_2)) + \sigma_{11}}{|\mu_1-\mu_2|^2\,|\mu_1|^2\,|\mu_2|^2} \\
& + \frac{|\mu_1-\mu_2|^2\,(a_{26}\,|\mu_1|^2\,|\mu_2|^2 - a_{16}\,|\mu_1|^2\,|\mu_2|^2)\sigma_{12} + a_{22}(|\mu_1|^2\,(-\mathbf{Im}(\mu_1)\mathbf{Im}(\mu_2) + \mathbf{Im}^2(\mu_2) + \mathbf{Re}(\mu_1-\mu_2)\mathbf{Re}(\mu_2))\sigma_{11}}{|\mu_1-\mu_2|^2\,|\mu_1|^2\,|\mu_2|^2} \\
& + \frac{|\mu_2|^2\,(\mathbf{Im}^2(\mu_1)\sigma_{11} - \mathbf{Im}(\mu_1)\mathbf{Im}(\mu_2)\sigma_{11} - \mathbf{Re}^2(\mu_1)\sigma_{11} + \mathbf{Re}(\mu_1)\mathbf{Re}(\mu_2)\sigma_{11} + |\mu_1-\mu_2|^2\,|\mu_1|^2\,\sigma_{22})}{|\mu_1-\mu_2|^2\,|\mu_1|^2\,|\mu_2|^2} \\
& + \frac{|\mu_1-\mu_2|^2\,(\mathbf{Im}^2(\mu_2)(\mathbf{Re}(\mu_1)\sigma_{12} + \mathbf{Im}(\mu_1)\sigma_{22}) + \mathbf{Im}(\mu_2)(\mathbf{Re}(\mu_1)\sigma_{12} + \mathbf{Im}^2(\mu_1)\sigma_{22} + \mathbf{Re}^2(\mu_1)\sigma_{22})}{|\mu_1-\mu_2|^2\,|\mu_1|^2\,|\mu_2|^2} \\
& + \frac{\mathbf{Re}(\mu_2)(\mathbf{Im}^2(\mu_1)\sigma_{12} + \mathbf{Re}(\mu_1)\mathbf{Re}(\mu_1+\mu_2)\sigma_{12} + \mathbf{Im}(\mu_1)(\sigma_{12} + \mathbf{Re}(\mu_2)\sigma_{22})))))}{|\mu_1-\mu_2|^2\,|\mu_1|^2\,|\mu_2|^2}
\end{aligned} \tag{3}
$$

## References


1. Brebbia CA, Domínguez J (1992) Boundary elements. An introductory course. WIT Press, Computational Mechanics Publications, Southampton
2. Eschenauer HA, Kobelev VV, Schumacher A (1994) Bubble method for topology and shape optimization of structures. Struct Optim 8: 42–51
3. Gallego R, Rus G (2004) Identification of cracks and cavities using the topological sensitivity boundary integral equation. Comput Mech 33
4. Garreau S, Duillaume P, Massmoudi M (2001) The topological asymptotic for the PDE systems: the elasticity case. SIAM J Control Optim 39(6): 1756–1778
5. Haataja J (2000) Matlab function for simulating a simple real-coded genetic algorithm. Center for Scientific Computing, Box 405, FIN-02101 Espoo. Internet: Juha.Haataja@csc.fi
6. Jackowska-Strumiłło L, Sokołowski J, Zochowski A (1999) The topological derivative method and artificial neural networks for numerical solution of shape inverse problems. Rapport de Recherche 3739, Institute National de Recherche en Informatique et en Automatique
7. Koguchi H, Watabe H (1997) Improving defects search in structure by boundary element and genetic algorithm scan method. Eng Anal Boundary Elements 19: 105–116
8. Kowalckzyk T, Fukukawa T, Yoshimura S, Yagawa G (1998) An extensible evolutionary algorithm approach for inverse problems. In: Tanaka M, Dulikravich GS (eds) Inverse problems in engineering mechanics, pp 541–550
9. Lekhnitskii SG (1981) Theory of elasticity of an anisotropic body. MIR Publishers, Moscow
10. Sokołowski J, Zochowski A (1998) Topological derivatives for elliptic equations. In: Proceedings of the inverse problems, control and shape optimization, pp 129–136
11. Sollero P (1994) Fracture mechanics analysis of anisotropic laminates by the boundary element method. PhD thesis, Wessex Institute of Technology
12. Stavroulakis GE (2001) Inverse and crack identification problems in engineering. Kluwer Academic Publishers, Dordrecht
13. Stavroulakis GE, Antes H (1998) Crack detection in elastostatics and elastodynamics. a BEM modelling-neural network approach. In: Tanaka M, Dulikravich G (eds) Inverse problems in engineering mechanics
14. Stavroulakis GE, Antes H (1998) Flaw identification in elastomechanics: BEM simulation with local and genetic optimization. Struct Optim 16: 162–175
15. Tanaka M, Nakamura M (1994) Application of genetic algorithm to plural defects identification. In: Bui H, Tanaka M, et al (eds) Inverse problems in engineering mechanics